Applied Catalysis A: General 308 (2006), p. 31-42

Structure–activity correlations in thin film model catalysts: CO hydrogenation on Rh/VO_x

Part I. The morphology, composition and structure of vanadia-supported and -promoted Rh particles upon oxidation and reduction

Simon Penner[a], Bernd Jenewein[a], Di Wang[b], Robert Schlögl[b] and Konrad Hayek[a]

* Corresponding author: E-mail address: simon.penner@uibk.ac.at

[a]Institut für Physikalische Chemie, Universität Innsbruck, Innrain 52a, A-6020 Innsbruck, Austria
[b]Department of Inorganic Chemistry, Fritz-Haber-Institut der Max-Planck-Gesellschaft, Faradayweg 4-6, D-14195 Berlin, Germany

Abstract

The combination of (high-resolution) electron microscopy and electron diffraction was applied to study the structural and morphological alterations of a number of Rh/VO_x-model systems upon oxidation and reduction, and to discriminate between different phenomena of metal–support interaction. Well-defined Rh particles (mean size 10–15 nm) were grown epitaxially on NaCl(001) surfaces and subsequently covered by layers of VO_x of varying thickness (0.07–2 nm), prepared by reactive deposition of V metal in 10^{-2} Pa O_2. Most films were covered with a stabilizing layer of amorphous alumina. The resulting model catalysts were subjected to an oxidative treatment at 673 K in O_2 for 1 h and to subsequent reduction in the temperature range 373–873 K.

While higher VO_x exposures (mean VO_x coverage ≥ 3 nm) favour the formation of crystalline V_2O_3 phases in partial epitaxial orientation to the Rh particles in the as-deposited state, lower exposures result in less ordered layers of cubic VO. Similarly, after a treatment in 1 bar O_2 at 673 K the oxidation states of vanadium vary between V^{5+} and V^{2+}, depending on the film thickness.

Decoration of Rh by reduced VO_x species was found to be the dominant feature of metal–support interaction upon reduction at low temperatures (T < 573 K), whereas at increasing reduction temperature the formation of distinct Rh–V alloys (V_3Rh_5, Rh_3V, V_3Rh and VRh, respectively) was observed. On a "VO_x/Rh/Al_2O_3" catalyst, prepared by depositing 1ML VO_x prior to Rh deposition alloy formation was not detected, and decoration of the metal particles was the dominant effect of reduction at 673 K. A counterpart to Rh/V "subsurface" or "surface" alloys, known to be formed on bulk Rh surfaces under similar conditions, could not be observed.

Keywords: Metal–support interaction; Rhodium; Vanadium; Alloy formation; Electron microscopy; Selected area electron diffraction

Preprint of the Department of Inorganic Chemistry, Fritz-Haber-Institute of the MPG *(for personal use only)* (www.fhi-berlin.mpg.de/ac)

1. Introduction

Vanadia-promoted and supported noble metals are well-known for their high activity in CO hydrogenation and for the selectivity in the formation of C_2-oxygenates like ethanol or acetic acid [1], [2], [3], [4] and [5]. Likewise, vanadium oxides promote CO_2 reforming with methane to synthesis gas [6], [7] and [8] and increase both the activity and the selectivity of supported noble metals towards N_2 in the reduction of NO with CO [9]. There is strong evidence that the critical steps of the above-mentioned reactions are favoured at the metal–support interface [3] and that vanadia-promoted catalysts are affected by metal–support interaction in a similar way as their TiO_2 promoted counterparts [10] and [11].

Several methods have been applied in order to bring metal and support in closer contact and, by increasing the contact area, to facilitate the formation of the key intermediates of those reactions. Suitable and well-used methods include the reduction at elevated temperature [12] and the preparation of ternary oxide phases. For example, calcination-induced metal–promoter interaction via $RhVO_4$-formation and -decomposition produces highly dispersed metallic Rh particles in contact with reduced vanadia species. The strong metal–oxide interaction leads to high selectivity to C_2 oxygenates and an increased CO conversion [3], [13], [14] and [15]. This concept can be generalized to other transition metal–oxide based systems (e.g. $RhNbO_4$, Rh_2MnO_4) [16]. Another pathway to increase the contact area between the metal and the vanadia support, and in turn to improve the ability to enter a state of strong-metal–support interaction (SMSI), is the use of thin epitaxially grown films as model systems [17]. In this particular case, metal nanoparticles, exhibiting regular polyhedral habits, are brought into intimate contact with the surrounding oxidic species by topotactic growth [18] and [19]. The resulting metal–oxide films provide a well-defined initial state to follow structural, morphological and compositional changes during catalyst activation and an eventual entering of an SMSI state.

In recent years, alloy formation in the (sub)surface region under reducing conditions has been found to account for pronounced structural alterations [18], [19], [20] and [21] and for changes in the catalytic activity [20], [21], [22] and [23] on bulk Rh surfaces in contact with VO_x. On "inverse" model catalysts (i.e. (sub)monolayers of V and VO_x deposited on a bulk Rh surface) some of the present authors observed a drastic increase in catalytic activity and a selectivity shift to methane in CO hydrogenation upon the formation of a subsurface alloy at 773 K and above [20] and [21]. V-subsurface alloys, being also formed on Pd surfaces [24], have been explored for their peculiar structural and chemical properties; e.g. the Rh(111)/V subsurface alloy exhibits enhanced activity in the dehydrogenation of methanol [21] and [22]. In a further study [25] we could show that surface and particularly subsurface alloys of V on a polycrystalline Rh surface are kinetically stable over an amazingly wide range of temperature and oxygen pressure, a property of importance for possible practical applications in the future.

The question now arises whether the catalytically active surface or subsurface alloy state is an intrinsic property of the Rh–V bulk, or if it can be also attained and stabilized in dispersed catalysts, consisting of small Rh particles in a vanadia environment, under reducing conditions. As outlined above, the use of well-defined thin film model systems is an adequate tool for this kind of studies, because thin film metal–oxide systems with Pt [26], [27], [28] and [29] and Rh [29] particles are prone to enter an alloy state upon reduction at comparatively low temperatures (> 573 K). This was confirmed in two previous studies on thin films containing Rh particles supported by pure vanadia [19] and [20], where different V–Rh alloys could be identified under different reduction conditions.

In the following we aim at a straightforward correlation between the microstructure and morphology on the one hand, and associated changes in the catalytic activity on the other hand, of vanadia-promoted Rh catalysts of different vanadia loading subjected to different oxidative and reductive treatments. In the present contribution (paper I), we want to focus on the

Preprint of the Department of Inorganic Chemistry, Fritz-Haber-Institute of the MPG *(for personal use only)* (www.fhi-berlin.mpg.de/ac)

identification of different features of metal–support interaction by electron microscopy and electron diffraction (structure and composition of vanadium oxide, decoration of free metal surface by reduced vanadia species, alloy formation, etc.), while their relation to changes in the catalytic properties in CO hydrogenation will be treated in the adjoining paper (paper II [30]).

2. Experimental

A high-vacuum chamber (base pressure 10^{-4} Pa) was used to prepare VO_x-supported and -promoted Rh samples. Rh particles were grown by electron-beam deposition at 623 K on two types of NaCl(001) substrates: vacuum-cleaved NaCl(001) single-crystal faces (0.25 cm^2), and in situ deposited NaCl films (surface area up to 100 cm^2). The latter were prepared by chemical vapour deposition of NaCl on polished Cu sheets at 360 K. The structure of metal particles and support is almost identical on the two substrates [17]. The NaCl(001) single crystal faces were cleaved in vacuo immediately before Rh deposition in order to avoid contamination. Rh metal (nominal thickness about 3 nm) was deposited from a wire wrapped around a tungsten rod while the film thickness was monitored by a quartz crystal microbalance. The samples were allowed to cool to room temperature and subsequently covered by a layer of crystalline vanadia of varying thickness, prepared by reactive deposition of V metal in 10^{-2} Pa O_2 at 623 K. A vanadium oxide coverage of 20–25 nm was sufficient to produce self-supporting samples for electron microscopy. The electron microscopy samples containing less vanadia and all the films for kinetic measurements were in addition covered with a supporting layer of amorphous alumina, prepared by reactive deposition of Al metal in 10^{-2} Pa O_2 (25 nm for electron microscopy samples, 500 nm for kinetic measurements). All films were subsequently floated and rinsed with water. The electron microscopy samples were dried and mounted on gold grids for electron microscopy, the catalyst samples were cleaned and mounted on quartz wool inside the reactor. For comparison, a pure Rh/Al_2O_3 catalyst was also prepared. The Rh/VO_x and $Rh/VO_x/Al_2O_3$ samples prepared in this way will be referred to as catalysts of type I.

In order to facilitate the discrimination between different mechanisms accounting for metal–support interaction, a second type of model catalyst (type II) was also prepared. In this case, approximately one monolayer (ML) VO_x (0.3 nm nominal coverage) was deposited on NaCl(001) at 623 K, before a Rh film of 3 nm nominal thickness was deposited at the same sample temperature. The resulting Rh particles were subsequently covered with a supporting layer of 25 nm alumina for electron microscopy, or with 500 nm alumina for kinetic measurements, respectively, at room temperature. Thereafter, the catalyst film (type II, $V/Rh/Al_2O_3$) was oxidized in 1 bar O_2 at 673 K for 1 h. Of course, compared with the catalysts of type I (containing Rh deposited on pure NaCl), the VO_x layer on catalysts II will block a considerable fraction of Rh metal surface area.

The structure and morphology of all electron microscopy films in the as-grown state and upon oxidative and reductive treatments were monitored by (high-resolution) electron microscopy ((HR)TEM) and selected area diffraction (SAED) with a Zeiss EM 10C and a Philips CM200 FEG, equipped with a Gatan imaging filter.

3. Results

Table 1 lists the studied Rh/VO_x catalysts. Four “type I” and one “type II” catalyst containing different amounts of VO_x are discussed: Rh/V_2O_3 (mean VO_x coverage 25 nm) (I-25); $Rh/V_2O_3/Al_2O_3$ (mean VO_x coverage 3 nm) (I-3); $Rh/VO_x/Al_2O_3$ (mean coverage 0.8 nm) (I-0.8); $Rh/VO_x/Al_2O_3$ (mean VO_x coverage 0.07 nm) (I-0.07); and $VO_x/Rh/Al_2O_3$ (mean VO_x coverage 0.3 nm) (II-0.3). For comparison, a purely alumina-supported sample (I-0), containing Rh particles of the same shape and size as I-3, I-0.8 and I-0.07, is also included.

Preprint of the Department of Inorganic Chemistry, Fritz-Haber-Institute of the MPG *(for personal use only)* (www.fhi-berlin.mpg.de/ac)

Table 1.

Characteristics of the studied Rh/vanadia thin film catalysts

Catalyst type	**Mean Rh thickness (nm)**	**VO_x coverage (nm)**	**VO_x phases present in the as-grown state**	**VO_x phases present after oxidation in 1 bar O_2 at 673 K**	**Phases present after high-temperature reduction (T > 573 K) in 1 bar H_2**
Type I					
I-25 Rh/VO_x	3.3	25	V_2O_3	V_2O_5	V_3Rh_5, VRh_3; VO, V_2O
I-3 $Rh/VO_x/Al_2O_3$	3.0	3	V_2O_3	V_2O_3	V_3Rh, VRh_3, VRh; VO
I-0.8 $Rh/VO_x/Al_2O_3$	3.0	0.8	VO	VO	Rh–V alloys at and above 673 K; VO
I-0.07 $Rh/VO_x/Al_2O_3$	3.0	0.07	Not detectable by TEM or ED	Not detectable by TEM or ED	Most likely Rh V alloys at and above 673 K; VO
I-0 Rh/Al_2O_3	3.0	0	–	–	Rh, Al_2O_3 (below 823 K)
Type II					
II-0.3 $VO_x/Rh/Al_2O_3$	3.0	0.3	VO	VO	Most probably Rh–V alloys above 673 K, VO

Alumina supports are always 25 nm thick.

3.1. The Rh/VO_x catalysts (type I)

3.1.1. The as-grown state

Fig. 1a shows the state of the Rh/V_2O_3 (I-25) catalyst after deposition. The Rh particles (mean particle size: 10–15 nm) exhibit polygonal outlines and are well discriminated from the vanadia support. The corresponding SAED pattern (Fig. 1b) confirms epitaxial growth of Rh on the former NaCl(001) template. The three-dimensional habits of the Rh particles have been determined previously to be mostly half-octahedral, half-tetrahedral and cuboctahedral [17]. Most particles expose a (100) plane perpendicular to the electron beam (which should equal the free metal surface primarily accessible to the reactants). Due to the relatively high Rh loading, coalescence of neighboured particles is occasionally observed. As the Rh particles were always prepared under the same conditions, their structure and morphology is similar in all catalyst films of type I discussed below, except for the (small) differences in the metal loading. The support shown in Fig. 1a consists of fairly regularly shaped V_2O_3 crystallites (average grain size about 6 nm), as determined previously [18]. The SAED pattern reveals partial epitaxy of V_2O_3 with respect to NaCl(001) and to regular side faces (mainly (111)) of the Rh particles. It is a pure superposition of the V_2O_3 and Rh patterns (some reflections are marked with arrows), indicating that no interaction between Rh and V_2O_3 had occurred during preparation. The secondary diffractograms developed around some intense Rh reflections are explained by double diffraction of the respective Rh(200) and (220) beams by the surrounding extended V_2O_3 grains.

The as-grown state of two selected $Rh/VO_x/Al_2O_3$ thin film catalysts with considerably less VO_x deposited (mean VO_x coverage 3 nm (I-3) and 0.07 nm (I-0.07)) is shown in Fig. 2a and b, respectively. An electron micrograph of the purely alumina-supported Rh film (I-0) is shown in Fig. 2c. The Rh particles of the catalysts shown in Fig. 2a–c are identical in size (but somewhat smaller than those of catalyst I-25 (Fig. 1a)), and more particles with square outlines, e.g. of half octahedral or cuboctahedral shape [17], are observed. As deduced from the micrograph in Fig. 2a and the SAED pattern shown in Fig. 2d, the 3 nm VO_x layer consists mainly of irregularly shaped grains (size about 5–10 nm) of crystalline V_2O_3. The diffractogram appears as a superposition of Rh, crystallized alumina and V_2O_3 patterns, the latter being in weak epitaxial relation with Rh (some reflections are marked with arrows). In catalyst I-3 (Fig. 2a), vanadium oxide grains are preferably attached to the Rh particles, leading to a rounding of the contour lines in comparison to catalyst I-0.07 (Fig. 2b). The small amounts of vanadia in catalyst I-0.07 are not directly detectable, neither in the electron micrograph nor in diffraction (Fig. 2b and e), and

Preprint of the Department of Inorganic Chemistry, Fritz-Haber-Institute of the MPG *(for personal use only)* (www.fhi-berlin.mpg.de/ac)

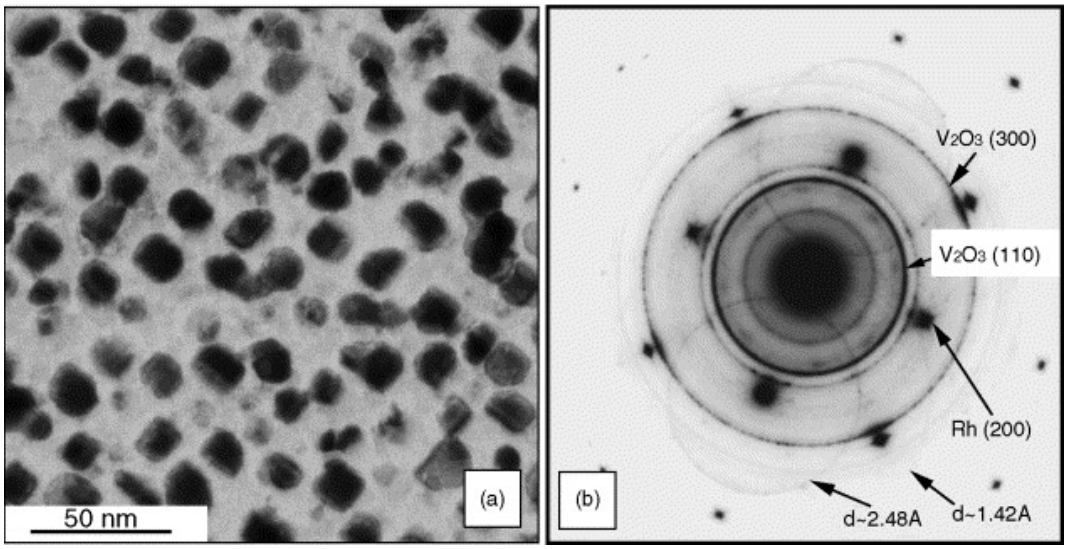

Fig. 1. The Rh (3.3 nm)/V_2O_3 (catalyst I-25) as deposited (a), corresponding SAED pattern (b).

the corresponding images are undistinguishable from those of the pure alumina-supported catalyst I-0 (Fig. 2c and f). However, the analysis of catalyst I-0.8 reveals that mainly VO is formed upon deposition in the (sub)monolayer range under the respective conditions (Table 1). In contrast to V_2O_3 and V_2O_5, cubic VO exhibits a porous microstructure of very small grain size which is hard to distinguish from that of the (partly crystallized) alumina support. (The Al_2O_3 support is amorphous in the as-grown state, but crystallizes readily in the electron beam of the microscope.)

3.1.2. Structure after oxidation at 673 K

After oxidation at 673 K in bar O_2 for 1 h of the Rh/V_2O_3 catalyst (I-25), the support is transformed into large grains of V_2O_5 and most Rh particles are still well aligned [18], although SAED patterns indicate that for some Rh particles a [011] zone axis is introduced (not shown here). On the contrary, V_2O_3 is the highest oxidation state observed on the alumina-supported catalyst I-3 (3 nm VO_x) after an equivalent oxidative treatment. The catalyst film I-0.8 (mean VO_x coverage 0.8 nm), treated in 1 bar O_2 at 673 K, is shown in Fig. 3a. The Rh particles appear well-shaped (from previous high resolution TEM [17] we know that only their immediate surface shell – about 1 nm thick – is oxidized under these conditions). The support exhibits a fine grain structure attributable to electron beam-crystallized γ-Al_2O_3. SAED patterns (Fig. 3b) reveal γ-Al_2O_3 and most probably also face-centered VO appearing not in epitaxial relation to the still well-aligned Rh particles. Higher vanadium oxides were not detected in this case.

3.1.3. Structure after reduction up to 873 K

3.1.3.1. Catalyst I-25

Fig. 4a shows a TEM overview micrograph of catalyst I-25 after reduction at 473 K. The Rh particles appear less ordered compared to the state after oxidation, and the support has acquainted the porous structure typical for VO [18]. The SAED pattern (Fig. 4c) shows rings of cubic VO together with broadened Rh spots. As outlined recently [19], further increase of the reduction temperature to 573 K results in the beginning formation of distinct V_3Rh_5 and Rh_3V alloy phases. Fig. 4b shows the film after reduction at 673 K, along with its diffraction pattern in Fig. 4d. The metal particles are now considerably increased in size compared to after reduction at 473 K (Fig. 4a), and the porous structure of the support persists. According to the diffraction pattern, metallic Rh is still present, and the support still consists mainly of cubic VO, but is partly further transformed into VO and V_2O phases with so far unidentified lattice structures (ui),

Preprint of the Department of Inorganic Chemistry, Fritz-Haber-Institute of the MPG *(for personal use only)* (www.fhi-berlin.mpg.de/ac)

as reported in the literature [31]. Table 2 lists the measured distances in relation to data from the literature [32], [33], [34] and [35].

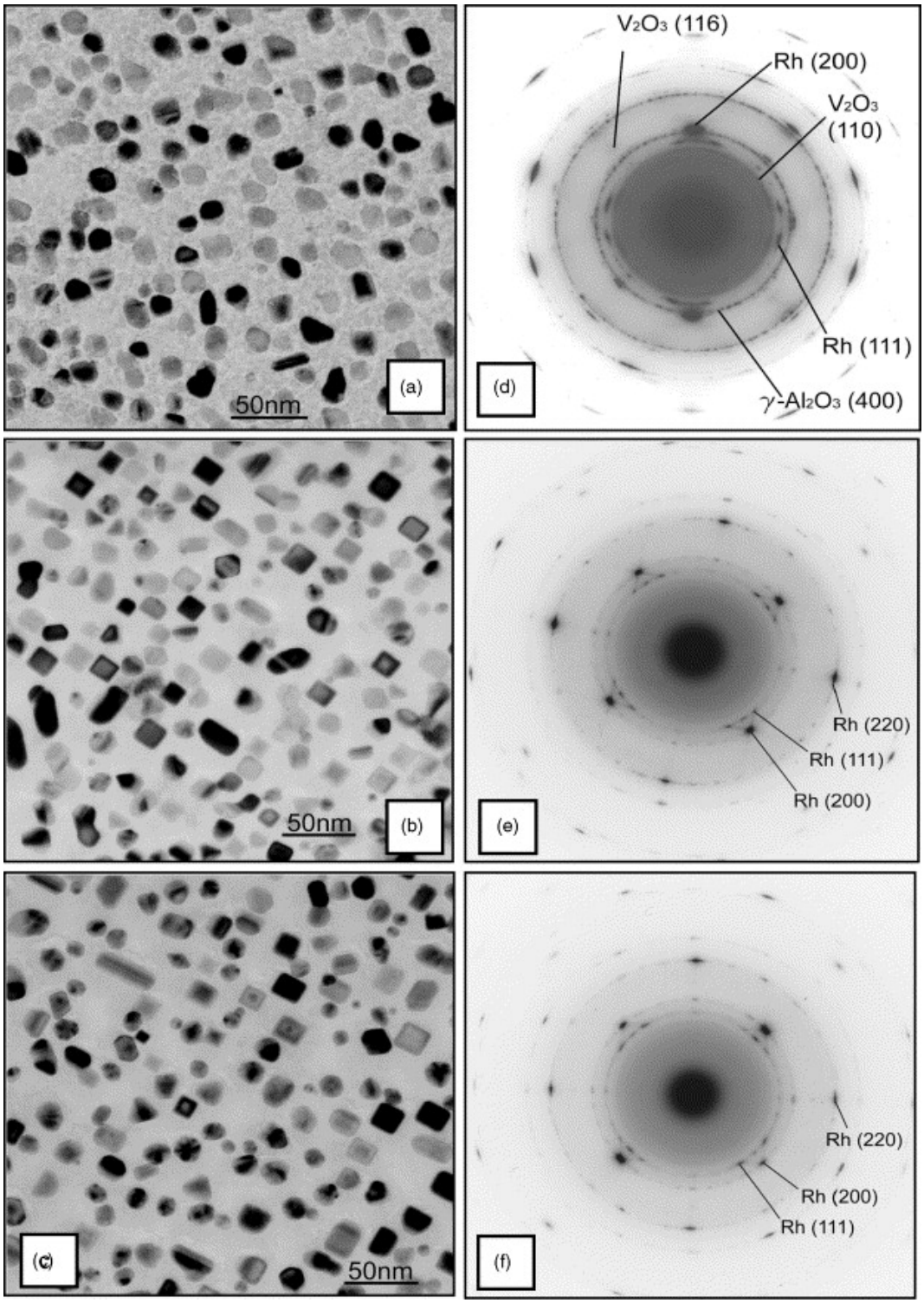

Fig. 2. Rh (3.0 nm)/VO_x/Al_2O_3 catalysts as deposited: (a) catalyst I-3, mean VO_x thickness 3 nm, (b) catalyst I-0.07, mean VO_x thickness 0.07 nm, (c) catalyst I-0, pure Rh/Al_2O_3. Corresponding SAED patterns in (d–f).

Preprint of the Department of Inorganic Chemistry, Fritz-Haber-Institute of the MPG *(for personal use only)* (www.fhi-berlin.mpg.de/ac)

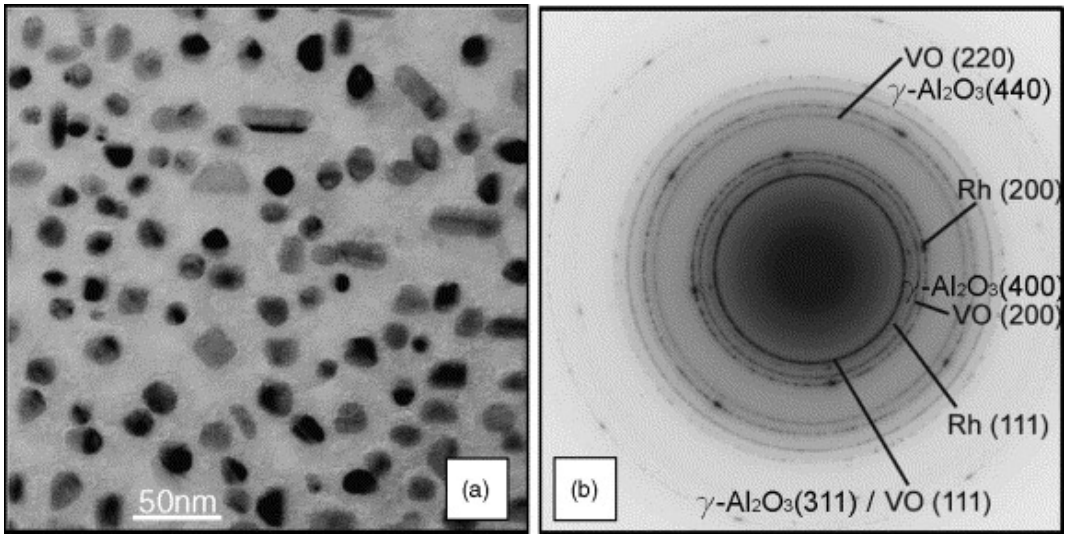

Fig. 3. Catalyst I-0.8 (Rh (3 nm)/VO_x (0.8 nm)/Al_2O_3) after oxidation at 673 K (a), and SAED pattern (b).

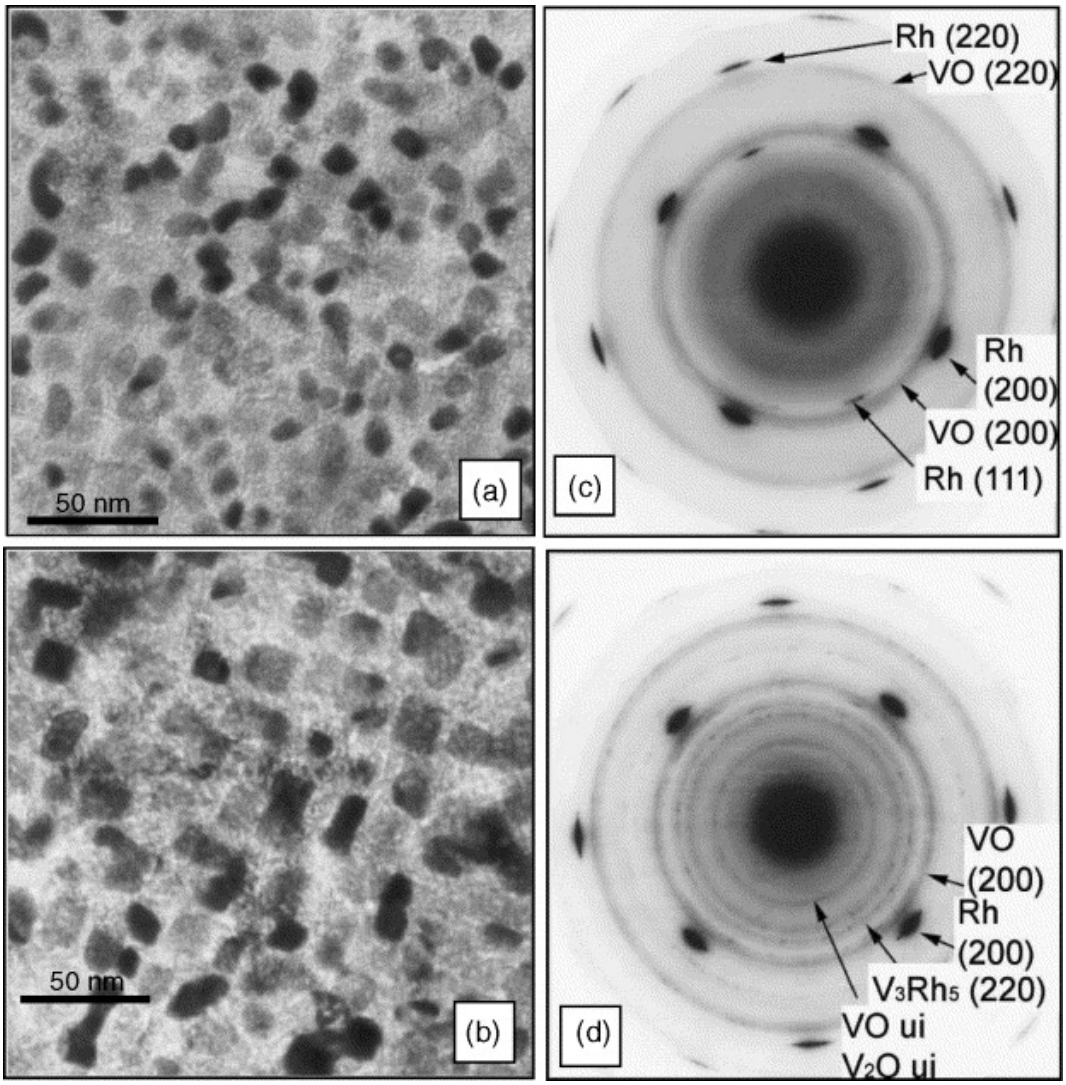

Fig. 4. Catalyst I-25 (Rh (3.3 nm)/V_2O_3 (25 nm)), oxidized at 673 K in 1 bar O_2 and reduced in 1 bar H_2 for 1 h at 473 K (a) and 673 K (b). Corresponding SAED patterns in (c) and (d).

Preprint of the Department of Inorganic Chemistry, Fritz-Haber-Institute of the MPG *(for personal use only)* (www.fhi-berlin.mpg.de/ac)

Table 2.

Interplanar distances d_{hkl} (Å) measured on catalyst I-25 after different reduction steps and possible correlation to cubic VO, monoclinic V_2O, VO/V_2O with unknown crystal structure (ui), cubic VRh_3 and orthorhombic V_3Rh_5

$d\ (hkl)_{exp}$	Assignment	
	Lattice plane	$d\ (hkl)_{theor}$
H_2 473 K, 1 h		
2.31	V_3Rh_5 (220)	[2.34]
2.03	VO (200)	[2.03]
1.76	V_3Rh_5 (240)	[1.76]
1.42	VO (220)	[1.43]
H_2 673 K, 1 h		
3.62	V_2O ui	[3.65]
	VO ui	
2.65	V_3Rh_5 (200)	[2.71]
	VO, V_2O ui	[2.70] [2.71]
2.47	VO, V_2O ui	[2.47] [2.48]
2.14	V_3Rh_5 (002)	[2.16]
	VRh_3 (111)	[2.15]
2.03	VO (200)	[2.03]
1.87	Rh (200)	[1.89]
1.78	V_3Rh_5 (240)	[1.76]
1.67	V_3Rh_5 (202)	[1.69]
1.44	VO (220)	[1.43]
1.40	V_3Rh_5 (400)	[1.36]
1.33	Rh (220)	[1.34]
H_2 773 K, 1 h		
3.65	V_2O ui	[3.65]
	VO ui	
2.65	V_3Rh_5 (200)	[2.71]
	VO, V_2O ui	[2.70] [2.71]
2.44	VO, V_2O ui	[2.47] [2.48]
2.16	V_3Rh_5 (002)	[2.16]
	VRh_3 (111)	[2.15]
2.05	VO (200)	[2.03]
1.87	Rh (200)	[1.89]
1.79	V_3Rh_5 (240)	[1.76]
1.65	V_3Rh_5 (202)	[1.69]
1.44	VO (220)	[1.43]
1.39	V_3Rh_5 (400)	[1.36]
1.33	Rh (220)	[1.34]
H_2 873 K, 1 h		
4.42	n.a.	
4.06	V_2O (−305)	[4.06]
3.86	V_2O (−206)	[3.88]
3.63	VO, V_2O ui	[3.65] [3.65]
3.01	V_2O (237)	[3.02]
2.67	V_2O ui	[2.70]
	VO ui	[2.71]
	V_3Rh_5 (200)	[2.71]
2.55	V_2O (464)	[2.58]
2.44	VO, V_2O ui	[2.47] [2.48]
2.34	V_3Rh_5 (220)	[2.35]
2.16	V_3Rh_5 (002)	[2.16]
	VRh_3 (111)	[2.15]
2.05	VO (200)	[2.03]
	V_3Rh_5 (221)	[2.05]
1.92	Rh (200)	[1.89]
1.78	V_3Rh_5 (240)	[1.76]
1.67	V_3Rh_5 (202)	[1.69]
	V_2O, VO ui	[1.68] [1.69]
1.56	V_3Rh_5 (042)	[1.58]
1.47	VO (220)	[1.43]
1.41	V_2O, VO ui	[1.43] [1.43]

Preprint of the Department of Inorganic Chemistry, Fritz-Haber-Institute of the MPG *(for personal use only)* (www.fhi-berlin.mpg.de/ac)

A further raise of the reduction temperature to 773 K does not lead to a considerable change of the catalyst structure (Fig. 5a and c). However, after reduction at 873 K the film is dominated by very large coalesced and probably thoroughly alloyed metal particles (Fig. 5b). The diffraction pattern (Fig. 5d) shows no Rh spots and is entirely composed of reflections of V_3Rh_5 and reduced VO_x species. Table 2 shows the assignment of the measured lattice distances to different structures.

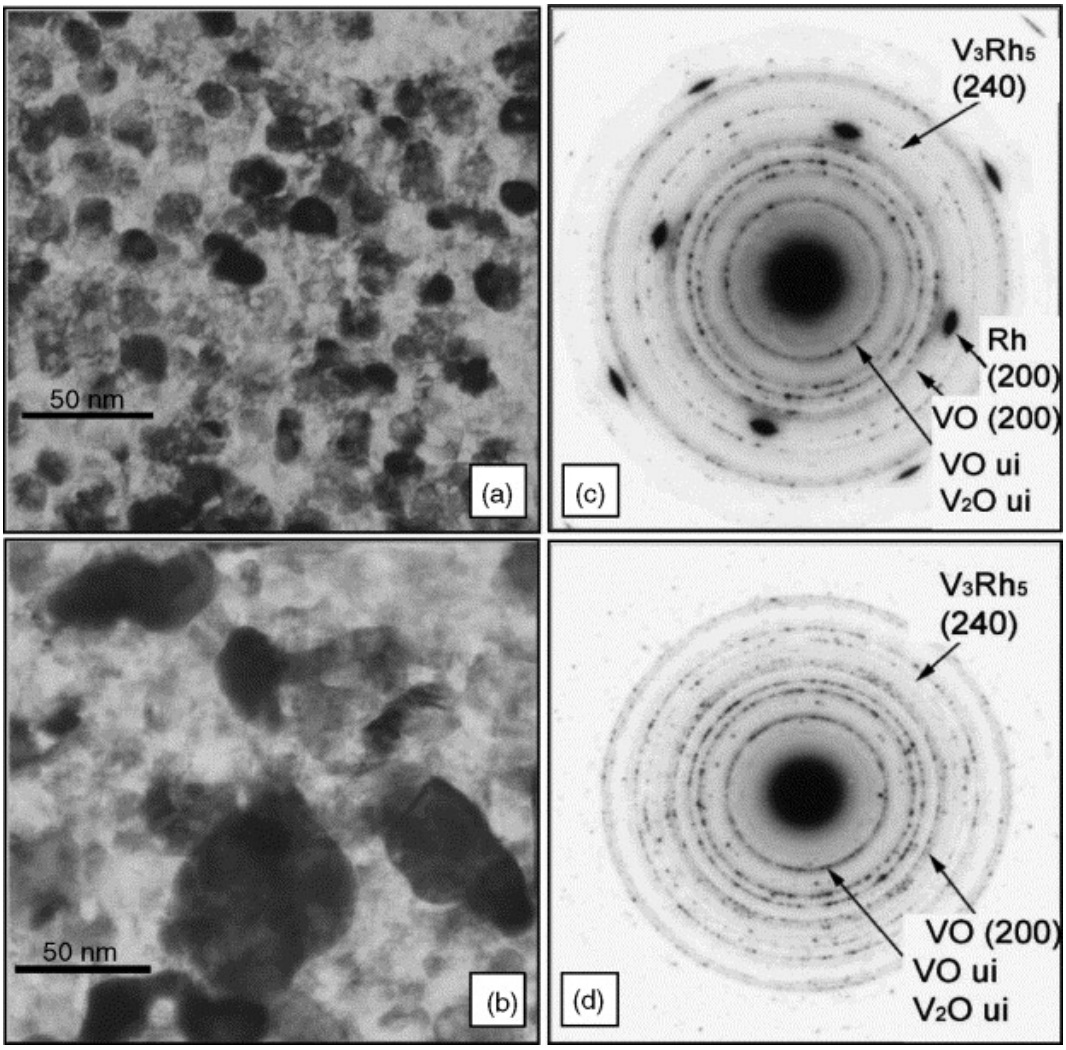

Fig. 5. Catalyst I-25 (Rh (3.3 nm)/V_2O_3 (25 nm)), oxidized at 673 K in 1 bar O_2 and reduced in 1 bar H_2 for 1 h at 773 K (a) and 873 K (b). Corresponding SAED patterns in (c) and (d).

3.1.3.2. The Rh/VO_x/Al_2O_3 catalysts I-0.07, I-0.8 and I-3.0

In contrast to purely VO_x-supported catalysts, the Al_2O_3-supported films containing less VO_x are not considerably changed by reduction at 573 K. Fig. 6a shows catalyst I-3 (VO_x coverage 3 nm) after a reductive treatment in 1 bar H_2 at 673 K for 1 h. The metal particles appear more rounded, but only slightly increased in size, and the SAED pattern (Fig. 6c) indicates the formation of distinct Rh–V alloy phases, as already observed previously under similar conditions [19]. We remember that in the as-grown state the Rh particles were closely surrounded by V_2O_3 grains. It is worth to emphasize that in this case mainly V_3Rh, VRh_3 and VRh are formed, in contrast to V_3Rh_5 in catalyst I-25, despite seemingly identical oxidation and reduction conditions. As outlined in Ref. [19], the dominant parameters leading to the different alloy structures are the crystallographic relation between Rh and the respective VO_x species and the nature of the VO_x support in the initial state in Reduction of catalyst I-0.8 (and equally of I-0.07) at 673 K leads to metal particles with rounded outlines, but strong signs of coalescence (Fig. 6b for catalyst I-0.8). The SAED pattern of catalyst I-0.8 (Fig. 6d) contains reflections from disordered Rh, clearly

Preprint of the Department of Inorganic Chemistry, Fritz-Haber-Institute of the MPG *(for personal use only)* (www.fhi-berlin.mpg.de/ac)

distinguishable as series of sharp rings, from substoichiometric vanadium oxides and, most likely, of several alloy phases. Only V_3Rh_5 particles could be clearly identified in HRTEM images, like the two particles shown in Fig. 7, exhibiting (220) lattice fringes [d_{theor}(220) = 2.34 Å]. A further reduction of the VO_x-promoted and hence Al_2O_3-supported catalysts at 773 K and above was impeded by beginning interaction of Rh and V with the alumina support and could therefore not be investigated further.

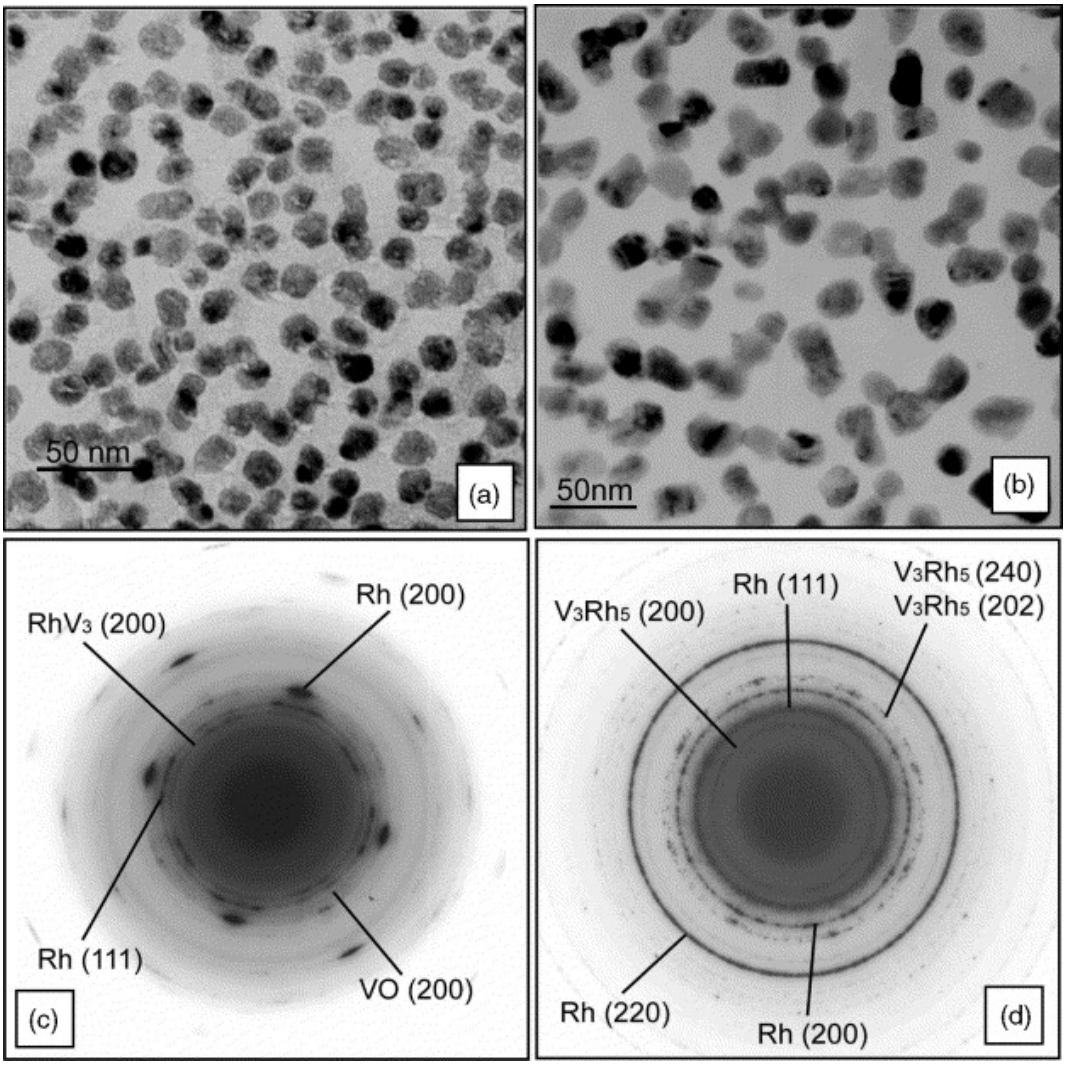

Fig. 6. Catalysts I-3 (a) and I-0.8 (b) oxidized at 673 K followed by reduction at 673 K in 1 bar H_2 for 1 h.

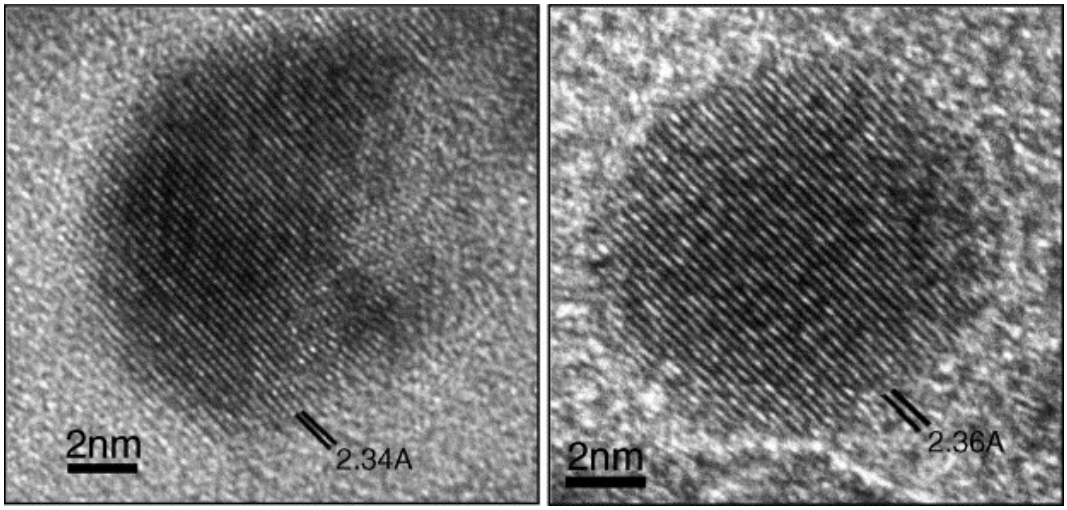

Fig. 7. HRTEM images of two V_3Rh_5 particles with (220) lattice fringes of catalyst I-0.8 (Rh (3 nm)/VO_x (0.8 nm)/Al_2O_3) after reduction at 673 K.

Preprint of the Department of Inorganic Chemistry, Fritz-Haber-Institute of the MPG *(for personal use only)* (www.fhi-berlin.mpg.de/ac)

3.1.4. Re-oxidation of I-25 after reduction at 773 K

Since catalyst activation usually involves oxidation–reduction cycles, we also focused on the question if and how the Rh/VO_x catalysts can be rejuvenated by re-oxidation after a high-temperature reduction (HTR) at 773 K. In view of the fact that oxidation at 723 K and above would cause complete oxidation of the Rh particles [17], connected with the loss of reversibility of their structural changes, a temperature of 673 K was set as an upper limit for re-oxidation. The electron micrographs of Fig. 8a and b and the corresponding SAED patterns (Fig. 8d and e) show catalyst I-25 after HTR (773 K) and subsequent oxidative treatments at 373 and 573 K, respectively. It is seen that these treatments are not sufficient to induce a change of the morphology or the structure of the films. In either case, the TEM images exhibit large, irregularly shaped alloyed particles on a structured and reduced VO_x support, while the diffraction patterns still resemble those after HTR, containing reflections due to V_3Rh_5, monoclinic V_2O and other substoichiometric VO_x species (V_2O and VO with yet unidentified crystal structure [31]). However, after oxidation at 673 K, the metal particles are drastically decreased in size, comparable to the size in the as-grown state (Fig. 1a) and have re-adopted more regular outlines, which points to a reversal of alloy formation. The VO_x support has developed larger grains and transformed into a V_2O_5-like structure (Fig. 8c). The diffraction pattern (Fig. 8f) still exhibits reflections from reduced vanadia species and V_3Rh_5 alloy, but strong reflections of pure Rh (marked by arrows) and from higher V oxides (especially V_2O_5) are also present. These results indicate that after reoxidation at 673 K under the given conditions the alloy phase is at least partially destroyed, and that the V_2O_5 support and the Rh particles are more or less re-established.

3.2. The VO_x/Rh/Al_2O_3 catalyst (type II)

3.2.1. As-grown state and structure after oxidation at 673 K

As mentioned above, this catalyst was prepared by depositing about 0.3 nm vanadia on NaCl(001), followed by deposition of about 3 nm Rh and of a supporting layer of 25 nm alumina. This implies that, compared to the other catalysts, considerable parts of the free, and therefore “active”, (100) surface of the Rh particles must be blocked by VO_x species.

Fig. 9a shows the catalyst film after oxidation at 673 K, with no considerable differences to the as-grown state being noted. The Rh particles are smaller, more densely packed and more irregularly shaped than those grown on pure NaCl(001) (cf. Fig. 1 and Fig. 2). The small fraction of VO_x is hardly detectable in overview TEM images, and the support is dominated by the fine structure of alumina. However, the SAED pattern (Fig. 9b) shows sharp rings (marked by arrows), attributable to cubic VO (besides γ-Al_2O_3), together with the reflections arising from the fcc Rh lattice. Hence, in this case, even after oxidation at 673 K, vanadium remains mainly in the V^{2+} state. The Rh particles appear in poor epitaxial relation with the underlying VO and the former NaCl support.

3.2.2. Structure upon reduction up to 673 K

After reduction up to 573 K, no structural changes of either the Rh particles or the oxidic support are observed in TEM or SAED. On the contrary, Fig. 9c shows that even after reduction at 673 K both the Rh particles and the support appear unchanged in the TEM, while the SAED pattern (Fig. 9d) still contains reflections from the Rh and the VO fcc lattices and from crystallizing γ-Al_2O_3. No signs of alloying were detected upon reduction at this temperature, which is in contrast to the findings on the Rh/V_2O_3 catalysts of type I discussed above. The only phenomenon pointing to metal–support interaction that is observed at this reduction stage is decoration and encapsulation of Rh particles by reduced VO_x species. Fig. 10 shows a HRTEM image of an encapsulated Rh particle exhibiting (200) lattice spacings. Again, further reduction

Preprint of the Department of Inorganic Chemistry, Fritz-Haber-Institute of the MPG *(for personal use only)* (www.fhi-berlin.mpg.de/ac)

at temperatures $T \geq 723$ K is impeded by beginning interaction between Rh, VO_x and the alumina support.

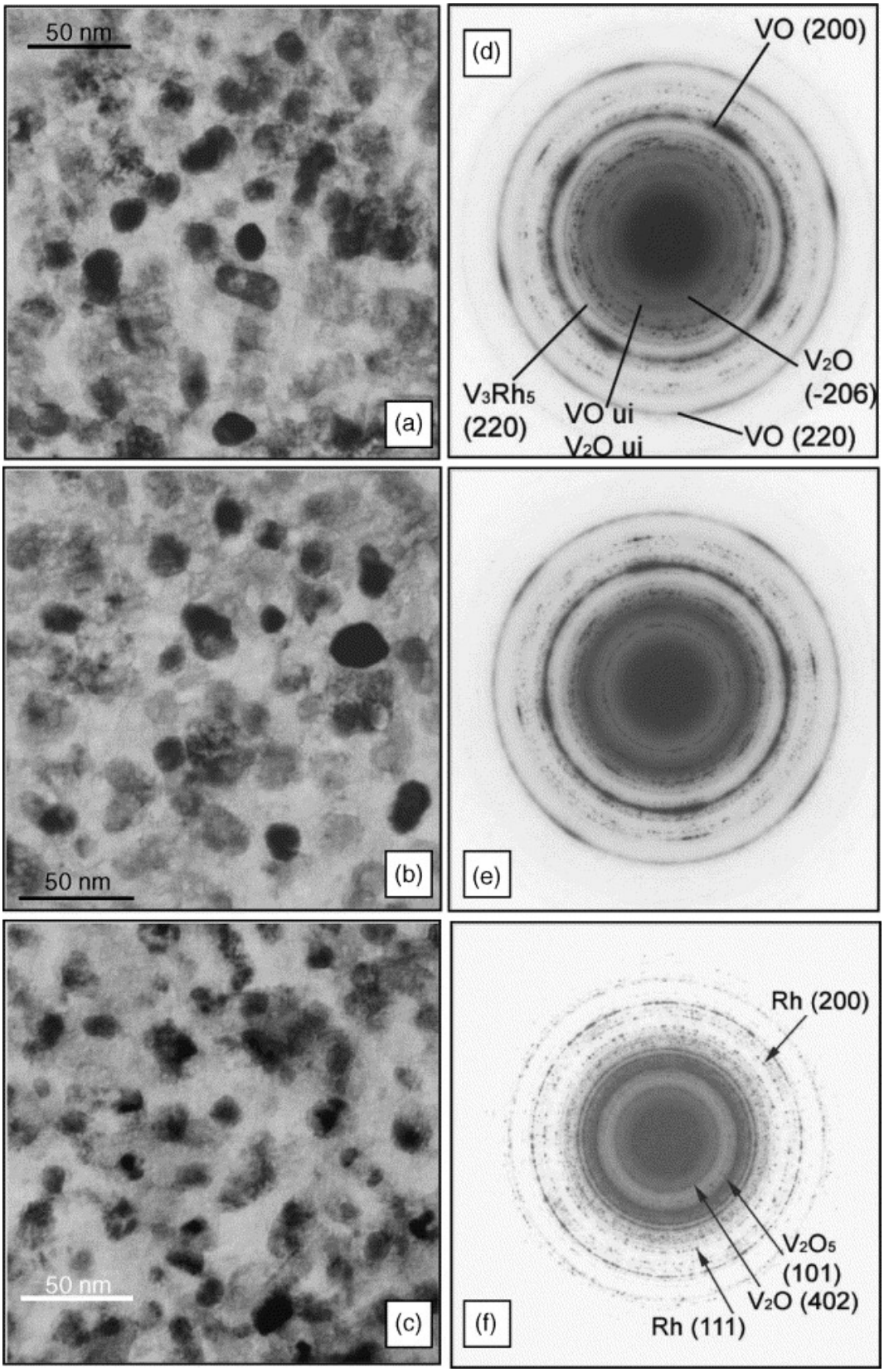

Fig. 8. Catalyst I-5 (Rh (3.3 nm)/V_2O_3) after reduction at 773 K in 1 bar H_2 followed by re-oxidation at 373 K (a), 573 K (b) and 673 K (c). The SAED patterns are shown in (d–f).

Preprint of the Department of Inorganic Chemistry, Fritz-Haber-Institute of the MPG *(for personal use only)* (www.fhi-berlin.mpg.de/ac)

3.2. The $VO_x/Rh/Al_2O_3$ catalyst (type II)

3.2.1. As-grown state and structure after oxidation at 673 K

As mentioned above, this catalyst was prepared by depositing about 0.3 nm vanadia on NaCl(001), followed by deposition of about 3 nm Rh and of a supporting layer of 25 nm alumina. This implies that, compared to the other catalysts, considerable parts of the free, and therefore "active", (100) surface of the Rh particles must be blocked by VO_x species.

Fig. 9a shows the catalyst film after oxidation at 673 K, with no considerable differences to the as-grown state being noted. The Rh particles are smaller, more densely packed and more irregularly shaped than those grown on pure NaCl(001) (cf. Fig. 1 and Fig. 2). The small fraction of VO_x is hardly detectable in overview TEM images, and the support is dominated by the fine structure of alumina. However, the SAED pattern (Fig. 9b) shows sharp rings (marked by arrows), attributable to cubic VO (besides γ-Al_2O_3), together with the reflections arising from the fcc Rh lattice. Hence, in this case, even after oxidation at 673 K, vanadium remains mainly in the V^{2+} state. The Rh particles appear in poor epitaxial relation with the underlying VO and the former NaCl support.

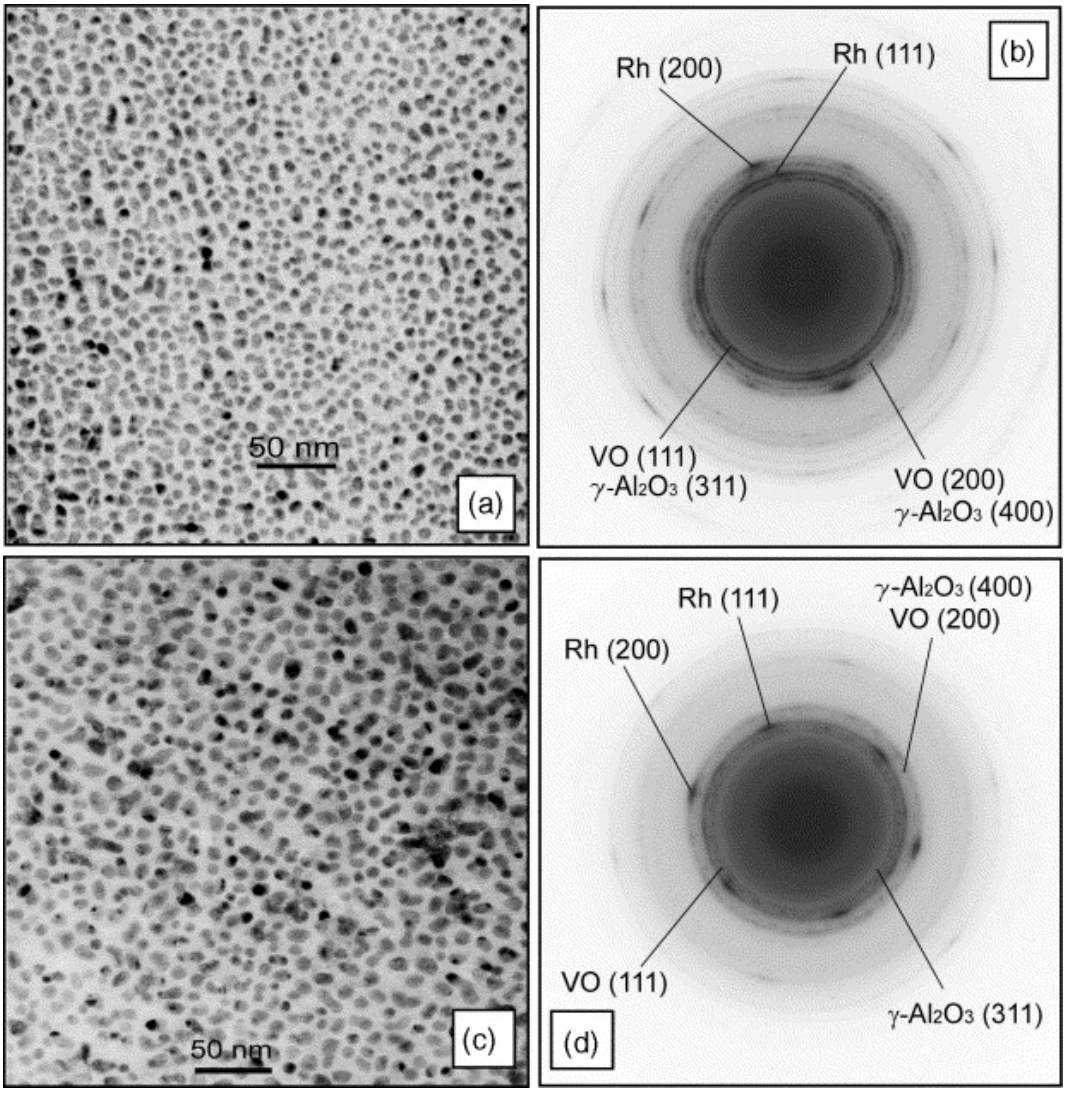

Fig. 9. Catalyst II-0.3 (V (0.3 nm)/Rh (3 nm)/Al_2O_3 (25 nm)) after oxidation at 673 K in 1 bar O_2 for 1 h (a) and SAED pattern (b) and after a following reduction at 673 K in 1 bar H_2 for 1 h (c), and corresponding SAED pattern (d).

3.2.2. Structure upon reduction up to 673 K

After reduction up to 573 K, no structural changes of either the Rh particles or the oxidic support are observed in TEM or SAED. On the contrary, Fig. 9c shows that even after reduction at 673 K both the Rh particles and the support appear unchanged in the TEM, while the SAED pattern (Fig. 9d) still contains reflections from the Rh and the VO fcc lattices and from crystallizing γ-Al_2O_3. No signs of alloying were detected upon reduction at this temperature, which is in contrast to the findings on the Rh/V_2O_3 catalysts of type I discussed above. The only phenomenon pointing to metal–support interaction that is observed at this reduction stage is decoration and encapsulation of Rh particles by reduced VO_x species. Fig. 10 shows a HRTEM image of an encapsulated Rh particle exhibiting (200) lattice spacings. Again, further reduction at temperatures $T \geq 723$ K is impeded by beginning interaction between Rh, VO_x and the alumina support.

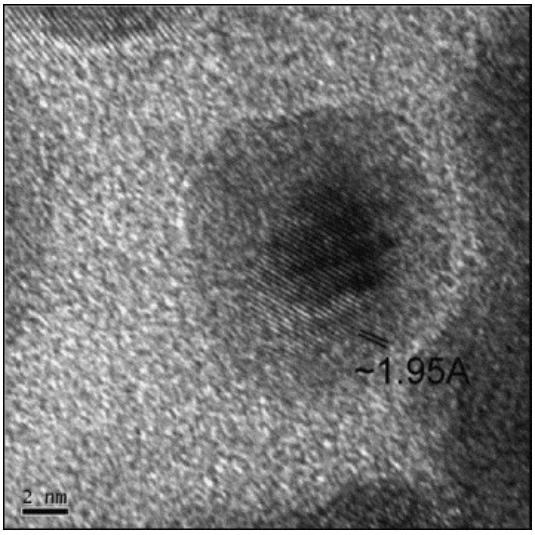

Fig. 10. HRTEM of an encapsulated Rh particle in catalyst I-25 after reduction at 673 K. The lattice fringes correspond to Rh(200) spacings.

4. Discussion

As in all catalysts studied the Rh particles are initially similar in structure and size, their different appearance upon oxidation and reduction must be caused by differing properties of the supporting/promoting oxide phase, such as stoichiometry and structure. We have seen that the oxidation state of V in the as-grown state depends on thickness of the VO_x layer. Under the given deposition conditions V_2O_3 is the main phase if the nominal VO_x coverage exceeds about 3 nm, whereas lower coverages lead only to VO formation. Similar holds for the state after oxidation at 673 K. V_2O_5 is only obtained on the VO_x supported catalyst, whereas V_2O_3 is observed on the promoted catalyst with the highest VO_x coverage (3 nm). On the other catalysts of low loading, only VO was observed even after oxidation at 673 K.

In contrast, upon reduction above 473 K cubic VO is the predominantly formed oxide phase, accompanied by V_2O and some other substoichiometric phases. It can be assumed that the decoration/encapsulation of the surface of Rh particles with low-grain size VO, formed already upon reduction at 473 K, is one of the major reasons for catalyst deactivation at the lower reduction temperatures (< 573 K).

In addition to the formation of reduced VO_x phases, alloy formation is the second dominant feature of the interaction between hydrogen, rhodium and vanadia in type I Rh/VO_x model systems. Under the given conditions, alloy formation is thermodynamically feasible, but its

Preprint of the Department of Inorganic Chemistry, Fritz-Haber-Institute of the MPG *(for personal use only)* (www.fhi-berlin.mpg.de/ac)

pathway depends on both the initial composition of the VO_x species in contact with the metal particles and the crystallographic relation between Rh and VO_x.

The structural and chemical changes after reduction are shortly summarized in Table 1 for all catalysts. The "initial state" is defined after oxidation at 673 K.

In vanadium oxide excess (catalyst I-25), the starting support phase after oxidation at 673 K is V_2O_5, partially epitaxially oriented with respect to the Rh particles, and upon reduction mainly V_3Rh_5 (and to a smaller extent V_3Rh, VRh_3 and VRh) is formed. The onset temperature of alloying is about 573 K [18] and [19]. This process is terminated after reduction at about 873 K. Then all Rh metal is consumed, resulting in large alloy patches (Fig. 5b).

On the other hand, the onset of alloy formation in the films of type I of lower V content (I-3 and I-0.8) is shifted to higher *T* (~673 K) (due to the low VO_x fraction alloy formation is not clearly detectable in catalyst I-0.07). The combination of Rh particles with an intimately connected epitaxial V_2O_3 shell, as in catalyst I-3, is found to result mainly in V_3Rh and VRh_3 formation. This is consistent with a model where V penetrates the Rh–V interface and forms a shell of a comparatively V-richer alloy before a further raise of the reduction temperature will equilibrate the V concentration inside the Rh particles [19]. (A similar behaviour was observed in corresponding experiments on ceria- and silica-supported Pt and Rh particles [26], [27], [28] and [29].)

Finally, no signs of alloying are detected upon reduction of catalyst II-0.3 up to 673 K, in contrast to the findings on the Rh/V_2O_3 catalysts of type I discussed above. At this stage only decoration and encapsulation of Rh particles by reduced VO_x species were observed. As is known from previous observations on other noble metal–oxide systems, this may be a consequence of the missing structural relation between the pre-deposited VO_x layer and the irregularly shaped metal particles.

5. Summary and conclusions

The combination of (high-resolution) electron microscopy and electron diffraction was successfully applied to study the structural and morphological alterations of several Rh/VO_x-model systems upon oxidation and reduction, and to discriminate between different phenomena of metal–support interaction. Well-defined Rh particles in contact with thin layers of VO_x, in part supported by a 25 nm film of alumina, were used as a starting point and oxidized at 673 K prior to reduction in hydrogen in the temperature range between 373 and 873 K. It could be shown that the stoichiometry and the local arrangement of the VO_x species surrounding the Rh particles depend on the thickness of the vanadia layer used as a promoter or support. Alloy formation (V_3Rh_5 or Rh_3V, respectively) sets in upon reduction at 573 K in catalysts of high V-loading, and at somewhat higher T on catalysts of lower loading. On the "$VO_x/Rh/Al_2O_3$" catalyst, prepared by depositing 1ML VO_x prior to Rh deposition, decoration of the metal particles was found to be the dominant effect of reduction at 673 K. A counterpart to Rh/V "subsurface" or "surface" alloys, known to be formed on bulk Rh surfaces under similar conditions, could not be observed.

Acknowledgement

Part of this work was supported by the Austrian Science Fund (Project S 8105).

Preprint of the Department of Inorganic Chemistry, Fritz-Haber-Institute of the MPG *(for personal use only)* (www.fhi-berlin.mpg.de/ac)

References

[1] G. van der Lee, B. Schuller, H. Post, T.L.F. Favre and V. Ponec, *J. Catal.* **98** (1986), p. 522.

[2] G. van der Lee, A. Bastein, J. van den Boogert, B. Schuller, H.-Y. Luo and V. Ponec, *J. Chem. Soc., Faraday Trans.* **83** (1987), p. 2103.

[3] S. Ito, S. Ishiguro, K. Nagashima and K. Kunimori, *Catal. Lett.* **55** (1998), p. 197.

[4] J. Kowalski, G. van der Lee and V. Ponec, *Appl. Catal.* **19** (1985), p. 423.

[5] T. Beutel, H. Knözinger, A.V. Siborov and V.I. Zaikovskii, *J. Chem. Soc., Faraday Trans.* **88** (1992), p. 2775.

[6] A.B. Boffa, A.T. Bell and G.A. Somorjai, *J. Catal.* **139** (1993), p. 602.

[7] M. Sigl, M. Bradford, H. Knözinger and M.A. Vannice, *Top. Catal.* **8** (1999), p. 211.

[8] A. Kohl, C. Linsmeier, E. Taglauer and H. Knözinger, *PhysChemChemPhys* **3** (2001), p. 4639.

[9] C. Neyertz, M.A. Volpe and C. Gigola, *Catal. Today* **57** (2000), p. 255.

[10] G.L. Haller and D.E. Resasco, *Adv. Catal.* **36** (1989), p. 173.

[11] R. Burch In: Z. Paál and P.G. Menon, Editors, *Hydrogen Effects in Catalysis*, Marcel Dekker, New York (1988), p. 347.

[12] T. Beutel, O.S. Alekseev, Y.A. Ryndin, V.A. Likholobov and H. Knözinger, *J. Catal.* **169** (1997), p. 132.

[13] S. Ito, S. Ishiguro and K. Kunimori, *Catal. Today* **44** (1998), p. 145.

[14] S. Ishiguro, S. Ito and K. Kunimori, *Catal. Today* **45** (1998), p. 197.

[15] S. Ito, C. Chibana, K. Nagashima, S. Kameoka, K. Tomishige and K. Kunimori, *Appl. Catal.* **236** (2002), p. 113.

[16] S. Ito, T. Fujimori, K. Nagashima, K. Yuzaki and K. Kunimori, *Catal. Today* **57** (2000), p. 247.

[17] G. Rupprechter, K. Hayek and H. Hofmeister, *J. Catal.* **173** (1998), p. 409.

[18] S. Penner, D. Wang, R. Schlögl and K. Hayek, *Thin Solid Films* **484** (2005), p. 10.

[19] S. Penner, B. Jenewein, D. Wang, R. Schlögl and K. Hayek, *PhysChemChemPhys* **8** (2006) (10), p. 1223.

[20] W. Reichl and K. Hayek, *J. Catal.* **208** (2002), p. 422.

[21] W. Reichl and K. Hayek, *Surf. Sci.* **537** (2003), p. 247.

[22] H.P. Koch, G. Krenn, I. Bako and R. Schennach, *J. Chem. Phys.* **122** (2005), p. 244720.

[23] G. Krenn, R. Schennach, J. Chem. Phys. 120 (12) (2004) 5729.

[24] C. Konvicka, Y. Jeanvoine, E. Lundgren, G. Kresse, M. Schmid, J. Hafner, P. Varga, Surf. Sci. (2000).

[25] W. Reichl and K. Hayek, *J. Catal.* **222** (2004), p. 53.

[26] S. Penner, D. Wang, D.S. Su, G. Rupprechter, R. Podloucky, R. Schlögl and K. Hayek, *Surf. Sci.* **532–535** (2003), p. 276.

[27] S. Penner, G. Rupprechter, H. Sauer, D.S. Su, R. Tessadri, R. Podloucky, R. Schlögl and K. Hayek, *Vacuum* **71** (2003), p. 71.

[28] D. Wang, S. Penner, D.S. Su, G. Rupprechter, K. Hayek and R. Schlögl, *J. Catal.* **219** (2003), p. 434.

[29] S. Penner, D. Wang, R. Podloucky, R. Schlögl and K. Hayek, *PhysChemChemPhys* **6** (2004), p. 5244.

[30] B. Jenewein, S. Penner, K. Hayek, following paper.

Preprint of the Department of Inorganic Chemistry, Fritz-Haber-Institute of the MPG *(for personal use only)* (www.fhi-berlin.mpg.de/ac)

[31] A. Mukherjee, *J. Less-Common Met.* **107** (1985), p. 89.

[32] Powder Diffraction File, International Center for Diffraction Data 1994. PDF Series 2, Sets 1-47, Pattern 35-361.
M. Arbuzov, *Inorg. Mater.* **17** (1981), p. 300 (Engl. Transl.).

[33] Powder Diffraction file, International Center for Diffraction Data 1994. PDF Series 2, Sets 1-47, pattern 27-1486.
R.M. Waterstrat and R. Dickens, *J. Less-Common. Met.* **31** (1973), p. 61.

[34] Powder Diffraction file, International Center for Diffraction Data 1994. PDF Series 2, Sets 1-47, pattern 17-63.
A. Dwight and T. Beck, *Trans. Am. Inst. Miner. Eng.* **215** (1959), p. 976.

[35] Powder Diffraction file, International Center for Diffraction Data 1994. PDF Series 2, Sets 1-47, Pattern 75-48.
H. Hartmann and W. Maessing, *Z. Anorg. Allg. Chem.* **226** (1951), p. 98.

Preprint of the Department of Inorganic Chemistry, Fritz-Haber-Institute of the MPG *(for personal use only)* (www.fhi-berlin.mpg.de/ac)